Monthly Notices
of the
ROYAL ASTRONOMICAL SOCIETY

MNRAS **454,** 3121–3133 (2015) doi:10.1093/mnras/stv2103

Mitigating systematic errors in angular correlation function measurements from wide field surveys

C. B. Morrison* and H. Hildebrandt

Argelander-Institut für Astronomie, Auf dem Hügel 71, D-53121 Bonn, Germany

Accepted 2015 September 8. Received 2015 August 7; in original form 2015 May 4

ABSTRACT

We present an investigation into the effects of survey systematics such as varying depth, point spread function size, and extinction on the galaxy selection and correlation in photometric, multi-epoch, wide area surveys. We take the Canada–France–Hawaii Telescope Lensing Survey (CFHTLenS) as an example. Variations in galaxy selection due to systematics are found to cause density fluctuations of up to 10 per cent for some small fraction of the area for most galaxy redshift slices and as much as 50 per cent for some extreme cases of faint high-redshift samples. This results in correlations of galaxies against survey systematics of order $\sim$1 per cent when averaged over the survey area. We present an empirical method for mitigating these systematic correlations from measurements of angular correlation functions using weighted random points. These weighted random catalogues are estimated from the observed galaxy overdensities by mapping these to survey parameters. We are able to model and mitigate the effect of systematic correlations allowing for non-linear dependences of density on systematics. Applied to CFHTLenS, we find that the method reduces spurious correlations in the data by a factor of 2 for most galaxy samples and as much as an order of magnitude in others. Such a treatment is particularly important for an unbiased estimation of very small correlation signals, as e.g. from weak gravitational lensing magnification bias. We impose a criterion for using a galaxy sample in a magnification measurement of the majority of the systematic correlations show improvement and are less than 10 per cent of the expected magnification signal when combined in the galaxy cross-correlation. After correction the galaxy samples in CFHTLenS satisfy this criterion for $z_{\rm phot} < 0.9$ and will be used in a future analysis of magnification.

Key words: gravitational lensing: weak – methods: data analysis – galaxies: photometry – galaxies: statistics.

1 INTRODUCTION

Measurements of the angular correlation of galaxies are powerful tools for probing the properties of galaxies and cosmology. Two-point correlation functions such as galaxy autocorrelation functions, weak gravitational lensing shear and weak lensing magnification are the basic observables of many current and future photometric surveys. However, the signals in these correlations can be contaminated by systematic errors arising from spatially inhomogeneous selections. Measurements of magnification bias especially suffer from these effects due to its small amplitude, even at small scales. While this paper takes systematics in magnification bias measurements as an example, the methods described herein will be useful for any small- to intermediate-scale, configuration-space correlation measurement.

Magnification has shown utility in measuring both mass and cosmology. Many of these measurements have been of magnification bias, the density change of galaxies due to lensing by intervening mass (Scranton et al. 2005; Hildebrandt, van Waerbeke & Erben 2009b; Bauer et al. 2011; Hildebrandt et al. 2011, 2013; Ford et al. 2012, 2014; Morrison et al. 2012). Other measurements have been also performed using magnitudes and sizes (Ménard et al. 2010; Bauer et al. 2011, 2014; Huff & Graves 2011; Schmidt et al. 2012). These measurements have been shown to be complementary to other probes of lensing of large-scale structure (Ménard & Bartelmann 2002; van Waerbeke 2010). Much of this complementarity is from the magnification signal coming for free, that is the same survey design and data reduction for weak lensing shear surveys also allows for magnification. Indeed, weak lensing magnification does not rely on shape measurements meaning that it will not suffer from the

* E-mail: cbmorrison@ucdavis.edu

same systematic errors. This comes at the cost of greater sensitivity to photometry errors and selection effects induced by survey systematics such as depth and point spread function (PSF) size. While magnification shows large sensitivity to these selection effects they will also be present in other correlation analyses including weak lensing shear though as second-order effects.

Much of magnification's and other correlations' mass and cosmological constraining power comes from measuring the signal at different radial distances and hence cosmic time. Selecting galaxies at a given distance is commonly done through colour and magnitude cuts or more generally photometric redshifts (photo-z). These selections should be uniform across the survey to maximize their scientific utility. However, variations in selection efficiency across the survey can induce spurious systematic errors into the correlations. This selection function can be caused by variations in survey depth, PSF full width at half-maximum (FWHM), extinction, and stellar density, for example. The different colour and photo-z selections cause the inhomogeneities to be different for each galaxy sample considered.

Current and future multi-epoch surveys will all suffer from such varying selection functions that will contaminate correlation measures. By leveraging the statistical power of the Canada–France–Hawaii Telescope Lensing Survey (CFHTLenS) data set, we investigate the effect of depth, PSF size, and extinction on galaxy density for several different galaxy samples. We find that these systematics can have an influence on the density, changing it by 10 per cent in some small fraction of the survey area for most samples and up to 50 per cent for some faint high-z samples. We then build an empirical, cosmology-independent method for reducing the effect of these systematics on correlation measurements. Techniques developed on CFHTLenS can be immediately used on other similar surveys such as the Red Sequence Cluster Lensing Survey (RCSLenS)[1] and the Kilo Degree Survey (KiDS)[2] as well as any survey using a data pipeline and survey strategy similar to CFHTLenS.

The paper is organized in the following way. The CFHTLenS data are presented in Section 2. Section 3 discusses angular systematics and how we relate those to the galaxy density. Results are presented in Section 4, where we show the galaxy densities as a function of the different systematics and the resulting spurious correlations. In Section 5, we develop our method for modelling and removing angular systematics with weighted random points. In Section 6, we show the results from applying this correction to the CFHTLenS data set. Finally, in Section 7 we summarize and give an outlook to applications within CFHTLenS and beyond.

2 DATA

The CFHTLenS data are described in Heymans et al. (2012), Erben et al. (2013), Miller et al. (2013) and Hildebrandt et al. (2012). Here, we will concentrate on the aspects of the data used in this analysis. CFHTLenS is a five band (*ugriz*) imaging survey consisting of 171 pointings of $\sim$1 deg^2. each observed in four different regions on the sky. Within each pointings the data are observed using 4–7 stepped dithers depending on the band pass. This observing strategy yields little overlap between pointings and CCDs. The unmasked area of the survey covers 117 deg^2. This area represents the strictest masking available for the survey. Reduced images and catalogues were produced using the THELI-pipeline (Erben et al. 2005). Objects are detected in the i band and the multicolour photometry is corrected for different PSF sizes between bands by performing a PSF homogenization (Hildebrandt et al. 2012).

Galaxies in this analysis are selected in two broad samples. The first, hereafter referred to as photo-z samples, are selected to have $19 < i < 24$ mag with photometric redshifts selected from BPZ (Benítez 2000) best-fitting redshift, z_b. The other samples, hereafter referred to as Lyman-break Galaxies (LBGs), are selected using the dropout criteria of Hildebrandt et al. (2009a) and have magnitude cuts of $23 < r < 24$ and $23.5 < i < 24.5$ for the u- and g-dropouts, respectively. These samples range from a total of $\sim$1 million galaxies in some of the photo-z samples to $\sim$30 thousand galaxies in the LBG samples.

For this analysis, we consider 11 different survey systematics in total. We consider the limiting magnitude, also referred to as the depth, in each of the five observed bands in the survey. The depths are estimated from the inverse variance images created during the THELI stacking process. We also use the PSF size in each of the five bands. We utilize the sizes as modelled for the PSF homogenization of Hildebrandt et al. (2012). The stellar density in the survey determines the fidelity of the PSF model. Small-scale variations cannot be captured due to the limited amount of information and the smoothing due to the functional fit. However, we do not expect the size of the stacked PSF to vary too much at small scales. As the last survey systematic, we consider galactic extinction which we estimate from the $E(B-V)$ values from the Schlegel–Finkbeiner–Davis (SFD; Schlegel, Finkbeiner & Davis 1998) dust map.

To encode the survey geometry and position dependence of the systematics, we utilize the spherical pixelization code STOMP (Scranton et al. 2002)[3]. This software allows us to pixelate the area of the survey and include complicated masking. We create constant resolution STOMP maps encoding the number of galaxies as a function of position for a galaxy sample. The number counts of galaxies are sample at pixels of 16 arcmin^2 and are summed or smoothed as need requires.. We also create constant resolution maps that encode variations in depth, PSF FWHM, and extinction. In Fig. 1, we show the i-band depth and seeing for an $\sim$1 deg^2 pointing in CFHTLenS. One can clearly see the effect of the dither pattern in the depth map. This pattern is repeated in the other CFHTLenS bands which leads to a strong correlation of the depth in the different bands. Note that the shallowest pixels are up to one magnitude shallower than the mean of the pointing. There are also smaller scale structures from pixel to pixel sensitivity differences. These variations change the number density and properties of the detected galaxies in the i band and also affect the colours of galaxies through the depth of the other four bands. The PSF size varies at much larger scales as shown in the right-hand panel of Fig. 1. This affects both the detection efficiency (in the i band) as well as the colour selection (in all bands) because the seeing influences the noise for small objects. Larger PSFs mean the detected surface brightness of galaxies decreases which affects errors and possibly also magnitude estimates through noise bias. Some of these colour differences are corrected in the PSF homogenization of (Hildebrandt et al. 2012), however, the noise variations associated with the varying PSF will remain and affect selections.

Fig. 2 shows the extinction for the same pointing seen in Fig. 1. The galactic dust causes a dimming and a reddening of galaxy colours. While CFHTLenS corrects for the reddening effect the dimming leads to a position-dependent depth variation with the same consequences as the depth variation due to the dithering

[1] http://www.rcslens.org
[2] http://kids.strw.leidenuniv.nl/
[3] http://code.google.com/p/astro-stomp

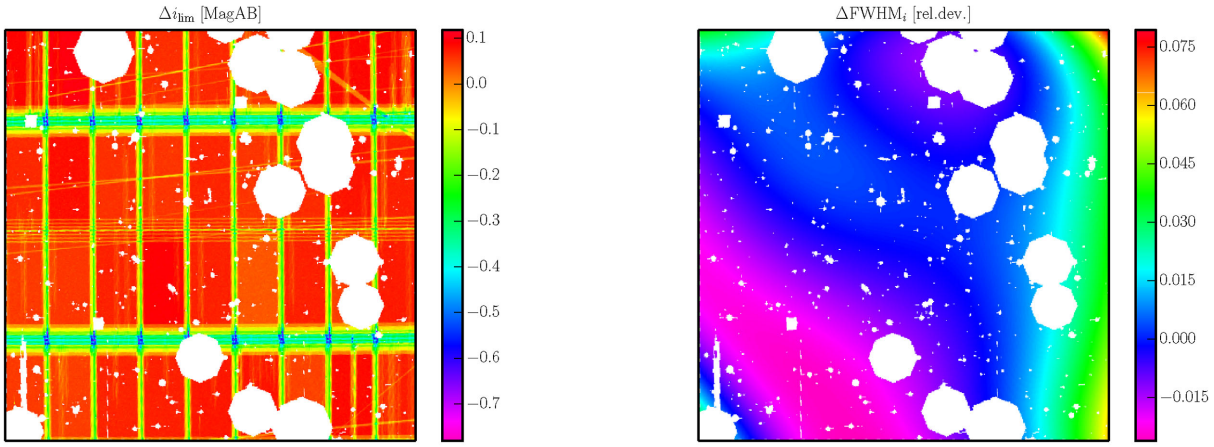

Figure 1. Map of the *i*-band depth (left) and PSF size (right) for one CFHTLenS pointing (∼1 deg^2). Each side of this plot is 1 deg^2. Values for the depth are relative to the mean of the field with the PSF size being fraction minus 1 relative to the mean. The depth shown is estimated from the inverse variance image produced during stacking. Red corresponds to deeper regions whereas green and blue correspond to shallower regions. The few blue pixels roughly one magnitude shallower than the red regions. The PSF size is estimated from the model used for the PSF homogenization of Hildebrandt et al. (2012). The colour scale shows large PSF in red/green and small PSF in blue/purple.

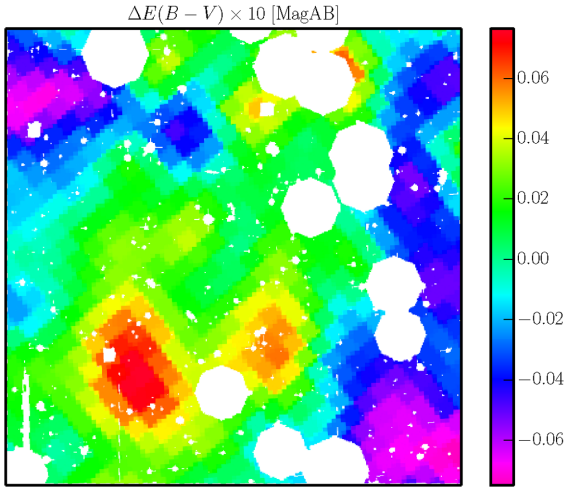

Figure 2. Map of $E(B-V)$ extinction relative to the mean of the pointing for the same CFHTLenS pointing as shown in Fig. 1. Red represents regions of high extinction, blue and purple regions of low extinction compared to the pointing mean. The values for the extinction are taken from the galactic dust maps of Schlegel et al. (1998) oversampled to the same resolution as the depth and seeing maps.

discussed above. The commonly used dust maps are also contaminated by light from high-redshift galaxies. This can lead to an unwanted physical correlation between the extinction correction and cosmic density.

We also encode the density of stars from two different star selections from Hildebrandt et al. (2012) and Miller et al. (2013). In the end, however, we do not utilize the stellar densities in this analysis due to difficulties with star–galaxy separation as described in Section 4.5.

3 GALAXY DENSITY ESTIMATES

Angular systematics in clustering measurements can arise from a position-dependent selection function caused by variations in instrumental and astrophysical quantities. The position-dependence gets imprinted on the data. Mathematically this can be written as

$$\delta(\boldsymbol{\theta}) = \frac{S(\boldsymbol{\theta})N(\boldsymbol{\theta}) - \langle S(\boldsymbol{\theta})N(\boldsymbol{\theta})\rangle}{\langle S(\boldsymbol{\theta})N(\boldsymbol{\theta})\rangle}, \quad (1)$$

where $\delta(\theta)$ is the galaxy overdensity at position $\boldsymbol{\theta}$, N is the true galaxy number count, and S is the sample-dependent selection. This factor can be significant, changing the density by as much as ∼50 per cent for certain samples in CFHTLenS. In the remainder of the paper we distinguish between δ and $\hat{\delta}$ where the latter quantity is our estimate from the CFHTLenS data, i.e. including shot-noise from the finite density of the survey. CFHTLenS is split up into individual pointings of roughly 1 deg^2 each. Within these pointings the data are observed using 4–7 stepped dithers depending on the band pass. This observing strategy yields little overlap between pointings and CCDs as can be seen in Fig. 1. In this figure, green and blue regions are chip gaps between CCDs which are significantly shallower than the mean of the survey by 0.2 mag. Further information on the dither pattern can be found in Erben et al. (2013). This limited overlap is a feature shared with many other current and near future surveys. This can lead to difficulties in the photometric calibration between pointings, inducing changes in galaxy densities related only to calibration issues. Analyses interested in scales larger than the pointing size need to be corrected for this effect. We instead remove variations that occur from pointing to pointing as we are interested in scales of the size of roughly a galaxy halo, much smaller than the CFHTLenS pointing size. Practically, we utilize the galaxy overdensity relative to the mean of the pointing to compute our statistics instead of the global survey mean. We similarly do this with each systematic considered, i.e. we relate the depth/seeing/extinction in a particular pixel to the mean of the depth/seeing/extinction in the pointing that the pixel resides in.

In Fig. 3, we compare the dependence of the measured overdensity on *i*-band depth before and after going from absolute (i.e. relative to the survey mean) to relative (i.e. relative to the mean of individual pointings) values. Both the galaxy density and *i*-band depth are estimated on a scale of 8 arcsec (we use this smoothing for all subsequent density estimates). Note the large increase in signal to noise between the two panels. While we show this only for the *i*-band depth, this is also true for the other systematic quantities.

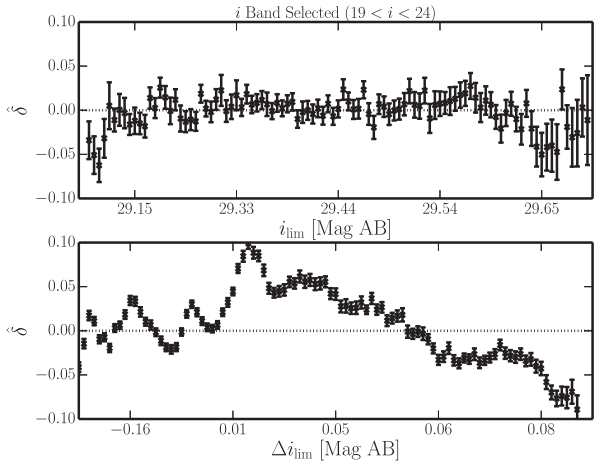

Figure 3. Galaxy overdensity $\hat{\delta}$ as a function of i-band depth for an i-band selected sample with $19 \leq i < 24$. The top panel shows the overdensity with respect to the survey mean galaxy density against the limiting magnitude (per pixel). The bottom panel shows the same but using galaxy density values relative to the mean in the individual pointings, averaged over the pointings as described in Section 3. Each data point corresponds to a non-contiguous survey area of 1 deg^2, that is from all pointings in the survey containing the systematic value range. The x-axis is plotted on a non-linear scale to allow for equal spacing between the data points to show the variations in density more clearly around the mean value of depth.

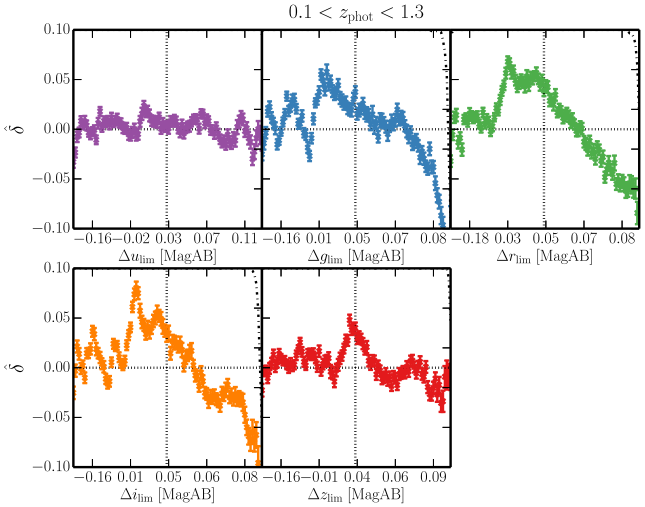

Figure 4. Plots of the galaxy overdensity $\hat{\delta}$ against the relative depth in the five CFHTLenS optical bands for the sample $0.1 < z_{\rm phot} < 1.3$. The dot–dashed line visible for large values of depth is the percentage of pointings (ranging from all 171 to 0) contributing to the density estimate of each depth bin.

This is probably due to the data reduction being done pointing-wise and the catalogues being created from running SEXTRACTOR (Bertin & Arnouts 1996) on the individual pointings rather than running the detection over the full survey at once. We will utilize this relative scaling for all plots in the remainder of the paper.

4 DEPENDENCE OF GALAXY DENSITY ON SYSTEMATICS

First, we compare the overdensity of galaxies in each sample against each of the systematics we consider separately. We bin the relative value of the systematic in ranges that represent equal area on the sky. We compute the values and error bars by spatially jackknifing over the pointings of CFHTLenS (171 in total) contributing to each bin. This jackknifing is done with weighting by area, that is pointings treated equally in the jackknife without regard for how much area they contribute to a particular systematic bin. The plots in the following sections show how the density can depend on the different systematics even for relatively bright, low-redshift galaxy samples.

4.1 *i*-band-selected sample

Before presenting results using photo-z and colour–colour selections, we show the density variations of a purely i-band-selected sample plotted against the i-band depth. The lower panel of Fig. 3 shows that the density as a function of relative i-band depth fluctuates in a complex way. For the deeper part data (right half of the lower panel of Fig. 3), we can understand this as the effect of Eddington bias leading to a monotonic decrease in density with increasing depth. This begins around the value of $\Delta i > 0.05$. In general, the Eddington bias in this case describes the asymmetric scatter of objects close to the noise limit. Since there are more faint than bright objects more objects scatter into the sample than out of the sample at the faint end. As the depth increases this effect becomes less important and density decreases. This is a general trend seen in the other bands as well. We have no such explanation for the shallower portions of the survey (left half of the lower panel of Fig. 3) though the trends seen there are likely due to complexities in the stacking and detection pipeline. While it is tempting to claim that the i-band-selected sample is completely independent of effects from the other five bands due to its selection relying on i-band only, this is not the case here as the survey mask used in this analysis uses information from all the observed bands and could introduce a selection dependent on the other bands. This can be seen in the next section where we plot these density fluctuations for the sample $0.1 < z_{\rm phot} < 1.3$ which is very similar to the i-band-selected sample.

4.2 Galaxy density versus depth

We now show the plots of galaxy density against the depth in all five bands for samples of galaxies in CFHTLenS selected in photometric redshift bins. In Fig. 4, we show the density variations of the $0.1 < z_{\rm phot} < 1.3$ sample against the depth. The dependence on i-band depth here is very similar to that of Fig. 3 showing an amplitude of up to ∼10 per cent. The other bands also show significant structure, however, some of this is expected to be redundant as the dither patterns are similar and therefore the depth varies in a similar way between the bands. Indeed, upon cross-correlating the depth maps of different bands with each other we find that the amplitude is roughly 50 per cent of the amplitude of autocorrelation of the individual band depth maps. For the low- and high-redshift galaxy samples that are a subsets of the sample shown in Fig. 4, the density variations in the u- and z-bands become more apparent as these bands are important for distinguishing high and low redshifts.

The cross-correlations of the galaxy positions for this sample against the depth maps are shown in the top-left panel of Fig. 5. Correlations are small here (<0.1 per cent) since no aggressive colour cuts are applied. The remaining panels of Fig. 5 show the same correlations for narrow photo-z slices. Much larger amplitudes of up to ∼0.3 per cent occur for some samples indicating the importance of the colour selection. Most of the correlations have an amplitude

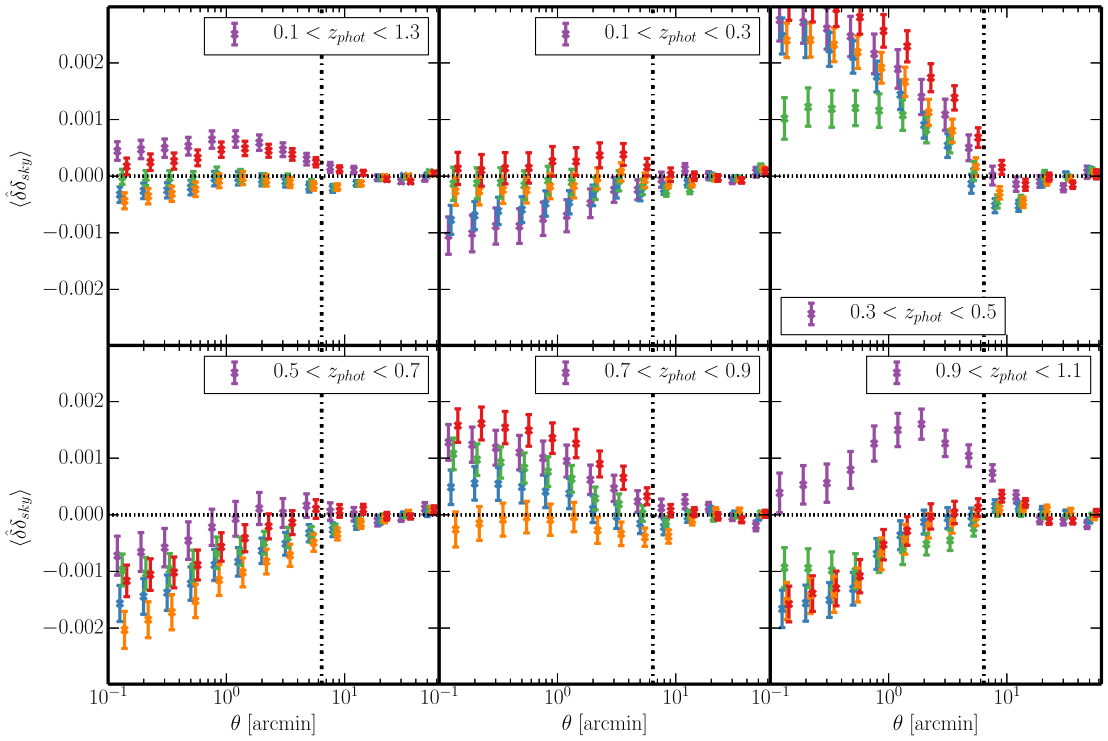

Figure 5. Angular cross-correlation functions between the observed galaxy density $\hat{\delta}$ and the survey depth $\delta_{\rm sky}$ in each band where purple $=u$, blue $=g$, green $=r$, yellow $=i$, red $=z$. We keep this convention throughout the paper. We plot all photo-z selected samples up to $0.9 < z_{\rm phot} < 1.1$ including the total sample of $0.1 < z_{\rm phot} < 1.3$ (top left). We neglect the $1.1 < z_{\rm phot} < 1.3$ for brevity though it is similar to the $0.9 < z_{\rm phot} < 1.1$ sample. The vertical dot–dashed line corresponds to the width of a MegaCam Chip.

of ∼0.1 per cent however and do not show significant structure as a function of θ. For the depth, we have information down to the scale of roughly an arcsecond and the autocorrelations of the depth maps do show power at these small scales. The galaxy samples show sensitivity to these small scales as some of the correlations (such as the $0.5 < i_{\rm phot} < 0.7$ sample) are not levelling off as they would if there was no dependence.

Two samples of note are the $0.3 < z_{\rm phot} < 0.5$ sample and the high redshift $0.9 < z_{\rm phot} < 1.1$ sample. The $0.3 < z_{\rm phot} < 0.5$ sample shows significantly higher cross-correlations against the depth maps – by about a factor of 2 – compared to the other samples. One would expect that this sample would be mostly free from systematics due to its low redshift and bright nature (i.e. similar to the $0.1 < z < 0.3$ sample). This is not the case as selecting this sample by photo-z relies heavily on information from the u band, which is shallower compared to the detection band, to distinguish it from the higher redshift selections. This is also true for higher redshifts such as $0.9 < z_{\rm phot} < 1.1$, which use a lot of information from the u- and z-bands for the redshift determination. Coupled with the faintness of the sample the $0.9 < z_{\rm phot} < 1.1$ sample exhibits a unique behaviour in that the cross-correlation against the u-band depth map is significantly different from the cross-correlations against the other bands, with an opposite sign and a large amplitude.

Fig. 6 shows the angular cross-correlation function between the density of the two LBG samples and the depth in the different bands. These galaxy samples show significantly larger density variations (not shown), up to five times that of the brighter photo-z-selected samples. Likewise we observe a roughly 10-fold increase in the amplitude of the cross-correlations for these samples. This drastic increase is to be expected given the faint nature of the LBG samples and their sensitivity to changes in the depth. The correlations that

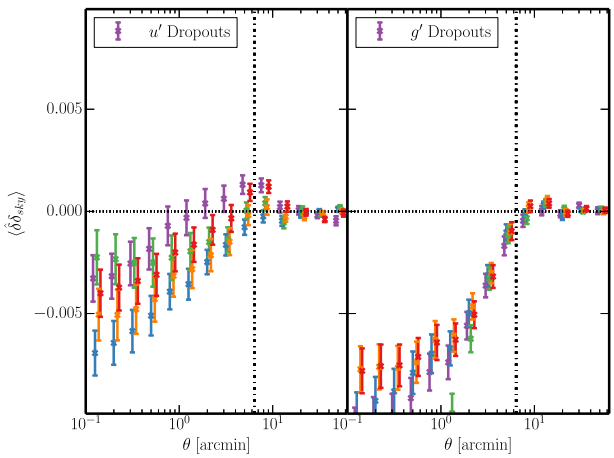

Figure 6. Similar to Fig. 5 but for samples of LBGs. Note the different y-axis range.

result from this are largely monotonic in θ with significant correlation at small and intermediate scales. These large correlations, in combination with the correlations from the other foreground samples, could lead to significant contamination of cross-correlation measurements between the different galaxy samples such as the ones used for magnification bias.

4.3 Galaxy density versus PSF size

In this section, we analyse the dependence of the galaxy density on the PSF size. As shown in Fig. 7 these density fluctuations are less pronounced compared to the trends seen with survey depth

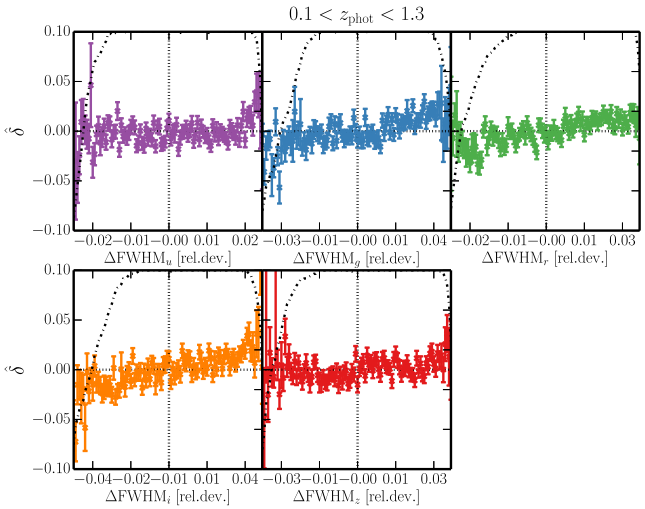

Figure 7. Plots of the galaxy overdensity $\hat{\delta}$ as a function of the PSF FWHM in the CFHTLenS optical bands for the sample $0.1 < z_{\rm phot} < 1.3$.

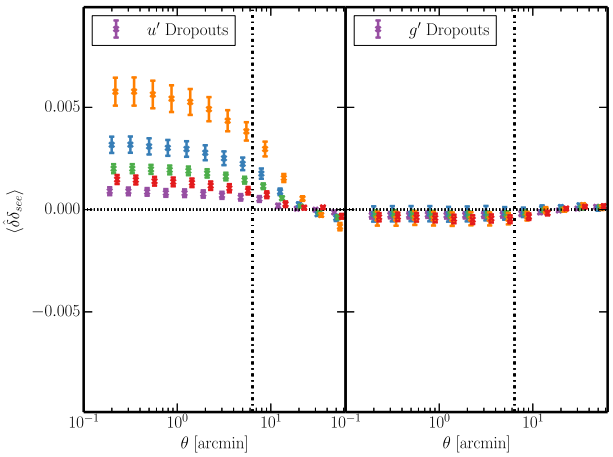

Figure 9. This figure is similar to Fig. 8 except we now show the cross-correlations of the densities of the two LBG samples against the PSF FWHM maps in the different bands.

(Section 4.2). They remain significant however with fluctuations of around 5 per cent at the highest. The strongest trend in the density is found when looking at the *i*-band PSF size. This is likely due to the fact that the *i* band is the detection band. This also suggests that the PSF homogenization that corrects for colour effects from different PSF sizes in each band (Hildebrandt et al. 2012) is working properly.

Correspondingly Fig. 8 shows the cross-correlation of the galaxy densities in the different samples against the PSF FWHM maps. The majority of the correlation seen here is flat at smaller scales ($\theta < 1$arcmin). This is not unexpected due to the fidelity of the seeing model we use from Hildebrandt et al. (2012). We do not expect the PSF size to be much of an issue at the smallest scales as it tends to vary much more smoothly compared to the depth. The amplitude we observe is as large as that of the depth and the correlation amplitude is almost always largest against the *i*-band PSF size map indicating that much of the correlation from the PSF is simply due to the detection process alone. Interestingly, the highest redshift slice appears to perform contrary to this trend with the correlation against the *z*-band PSF FWHM map being largest. This again suggests that the higher redshift samples are more sensitive to the *z* band through the redshift selection.

The results are mixed for the LBGs as shown in Fig. 9. The *u* dropouts show large correlation amplitudes roughly equal in amplitude to the correlations against the depth maps. However, the

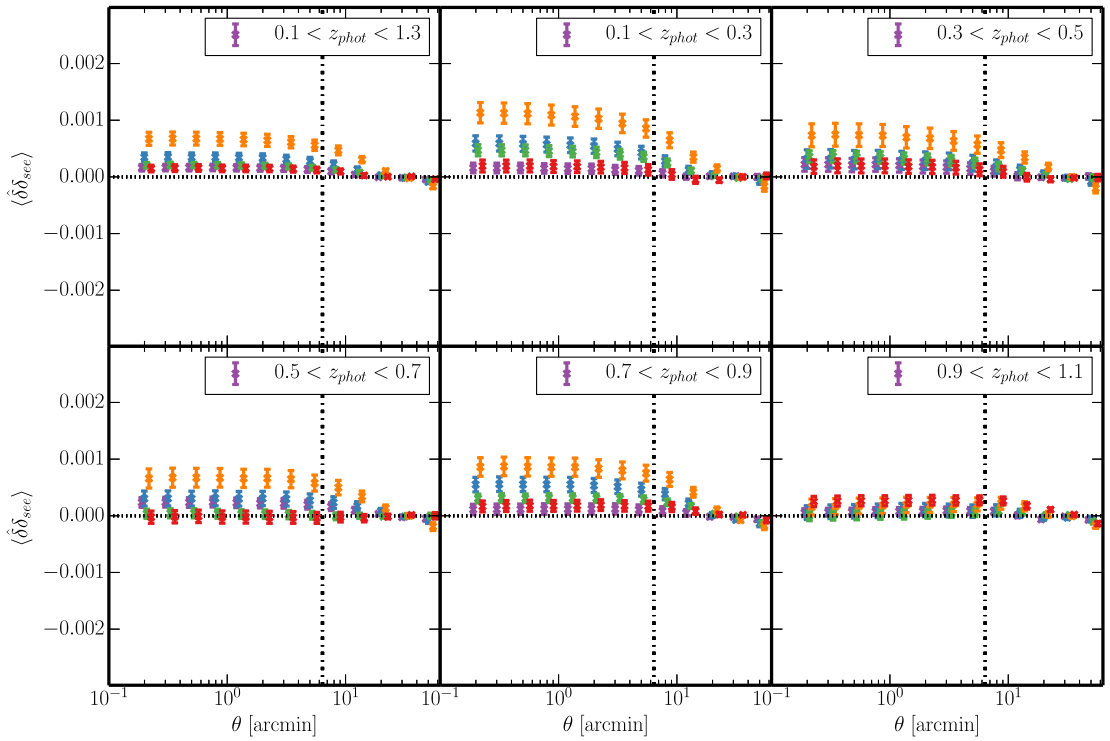

Figure 8. This figure is similar to Fig. 5 except we now show the correlations against the PSF FWHM in each of the five bands.

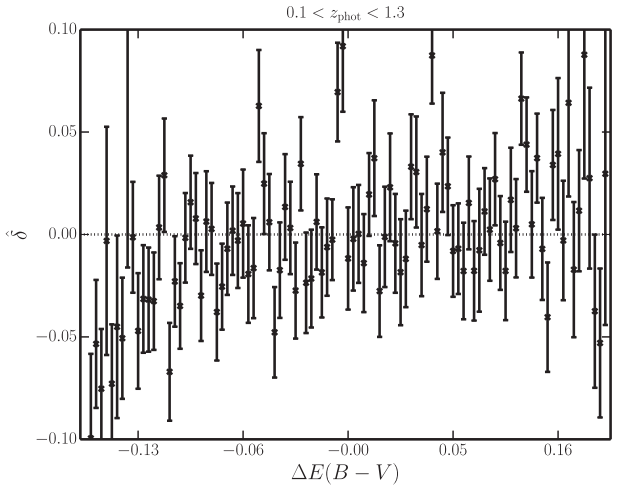

Figure 10. Galaxy overdensity $\hat{\delta}$ against the relative $E(B-V)$ value from the SFD dust maps for the sample $0.1 < z_{\rm phot} < 1.3$.

g dropouts, which have the largest cross-correlation amplitudes to the depth overall, show very little correlation to the PSF size, with the amplitude being an order of magnitude lower than that of the *u* dropouts. We do not have an explanation for this surprising behaviour.

4.4 Galaxy density versus extinction

Milky Way dust can also introduce spurious correlations into galaxy samples. High-redshift galaxies observed through galactic dust will have their colours reddened and thus their selection will change as the dust opacity changes. This effect usually is corrected using the SFD (Schlegel et al. 1998) dust maps or similar data, modifying the galaxy sample's colours based on the amount of dust measured at a given location. However, these corrections cannot account for changes in the noise properties of the detected galaxies or – equally important – any galaxies not detected due to the extra opacity. SFD and similar maps of dust opacity are also contaminated by high-redshift galaxies as the infrared emission used to determine the dust opacity is contaminated by the emission from the cosmic infrared background (CIB; Schmidt et al. 2015). In addition to this, we do not have access to data describing the small-scale fluctuations of dust extinction. Indeed, the small-scale structure of galactic extinction is an ongoing topic of research (Planck Collaboration XI 2014).

Fig. 10 shows the density of the $0.1 < z_{\rm phot} < 1.3$ sample plotted against the amount of extinction relative to the mean of the pointing. The density variation shows a trend from small values to large with the density increasing with extinction. The reason is probably again Eddington bias as discussed in Section 4.1. After correction for the reddening the main remaining effect of dust is that it changes the depth of the data. This systematic mostly affects the lower redshifts as their bluer colours make them more sensitive to dust absorption.

The cross-correlations of the galaxy densities in different redshift slices against the dust map are shown in Fig. 11. Large amplitudes are found suggesting that the effect of dust changing the noise properties of galaxies is at least as important as the effects from varying depth and seeing. Surprisingly, all samples show a significant anticorrelation at large scales (∼50 arcmin) of the order of ∼0.05 per cent.

In Fig. 12, we show the correlations of the densities of the LBG samples against the extinction maps. Unlike for cross-correlation against the depth maps, where the LBG samples showed amplitudes larger by an order of magnitude compared to the photo-*z* selected samples, we find that the amplitude of the cross-correlation of the extinction with the LBG densities is within a factor of 2–3 compared

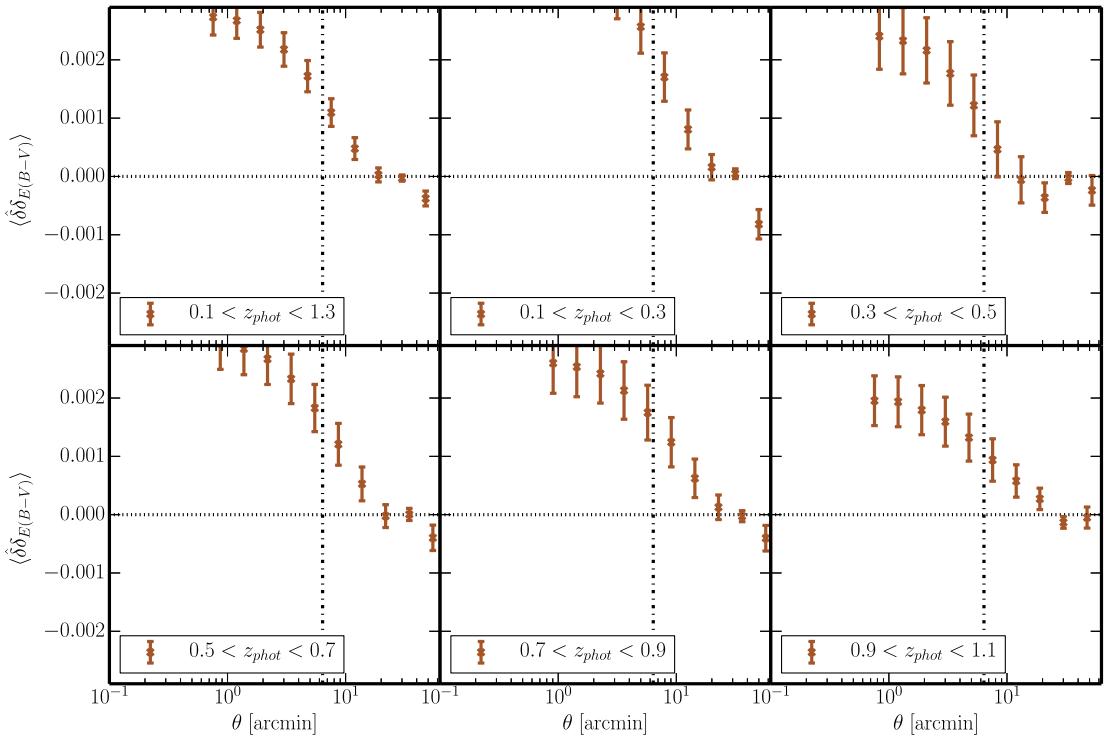

Figure 11. This figure is similar to Fig. 5 except we now show the correlations of galaxy density at different redshifts against the galactic extinction $E(B-V)$ from the SFD dust maps (Schlegel et al. 1998).

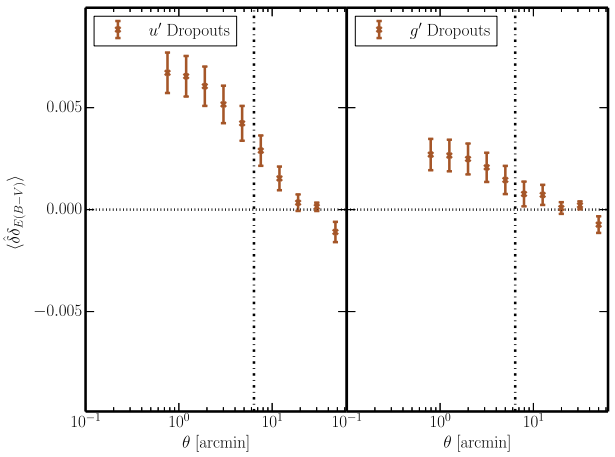

Figure 12. This figure is similar to Fig. 11 except we show the correlation for the *u*- and *g*-dropout samples.

to the amplitude for the photo-*z*-selected samples. While the LBG samples have the reddest colours of any sample we consider, making them less sensitive to extinction, they rely on non-detections in the bluer filters for their selection making them sensitive to the extinction.

4.5 Galaxy density versus stellar density

The density of stars can also impact the selection function of galaxy samples (see e.g. Ross et al. 2012). Two effects that can cause this are problems with star–galaxy separation and stellar light haloes obscuring galaxies and changing their colours. Poor star–galaxy separation causes stars to be miss-identified as galaxies and vice versa. The effect is to contaminate the galaxy correlation signal with the stellar correlation and suppress the amplitude. Galaxies observed through stellar haloes in dense stellar fields also have their densities and correlations affected.

We attempt to quantify the amount of correlation between a stellar sample, galaxies in CFHTLenS, and the other systematics, however we find very inconsistent results based on how the stellar sample was selected either through colour (Hildebrandt et al. 2012) or purely shape-based methods (Miller et al. 2013). These different stellar catalogues correlate very differently against a given galaxy sample for all magnitudes of the stellar sample.

We employ an alternative method to test the effect of stellar haloes by adding larger masks around each of stars from both stellar samples. The masks are chosen to reject areas 100 times the area of detected stellar objects. Little change is observed in the amplitude of the cross-correlations at all scales. The higher redshift samples show no change with the new more aggressive stellar masking. This and the observed flatness of the angular correlation function suggest that the cross-correlation of the stellar samples and the galaxy samples is dominated by stellar contamination in the galaxy sample rather than the previously mentioned halo effect. The stellar contamination is part of a larger issue of star–galaxy separation that we do not address in this paper.

These inconclusive results are the reason why we do not consider stellar density as an additional systematic effect in our analysis in the following. More generally, any systematic that cannot be mapped with sufficient accuracy is problematic and cannot be analysed/removed with our approach. The whole procedure relies on detailed two-dimensional maps of the systematics which are not readily available for the stellar density.

5 MODELING AND REMOVING ANGULAR SYSTEMATICS

Angular systematics from position-dependent selection functions can be a significant portion of the observed signal when performing a correlation analysis. In order to remove such spurious signals, we employ an empirical method of creating weighted random catalogues from the data.

Spectroscopic surveys already employ a weighting of galaxies to correct for changes in sensitivity and selection function (e.g. Le Fèvre et al. 2005; Ross et al. 2012; Newman et al. 2013). These weightings are both analytically and empirically determined and enable the use of random galaxy samples that, when used in correlation estimators, remove much of the systematic variation from the data set. This is not as commonly done with photometric surveys as selections are thought to be more homogeneous. As we have shown above this is not the always the case.

Simulating the selection effects would be one way to account for this. However, selections that use photometric redshifts estimated from non-linear fitting are quite complex and difficult to simulate. We can, however, remove such systematics from photometric samples using a fully empirical method. Empirical modelling of systematic effects in photometric correlations has been used in Fourier-space for large-scale BAO analyses (Ho et al. 2012; Leistedt et al. 2013; Leistedt & Peiris 2014). Here, we describe a method that works in configuration space and at small scales (∼1 arcmin). We estimate weight maps for random points from the data itself using a mapping from measured instrumental/astrophysical quantities to observed galaxy density. Here we consider the effects of depth in five bands, PSF size in five bands, and galactic extinction totalling in 11 survey systematics for CFHTLenS. This method can only work if the quantities used are not intrinsically correlated with the observed samples, i.e. through a process that we would like to measure. As long as we limit ourselves to instrumental and galactic quantities, extragalactic measurements should not be affected.

5.1 Weighted random points

Weighted random points can be used in order to remove position-dependent systematics induced by a varying selection function. This approach attempts to model and remove the systematics by mimicking the selection function's effect through random points that follow the under- and overdensities. These random points are used in the Landy & Szalay (1993) correlation estimator which can be written as

$$\hat{w}(\theta) = \frac{D_1D_2 - D_1R_2 - R_1D_2 + R_1R_2}{R_1R_2}, \quad (2)$$

where D_1D_2 are the number of pairs as a function of angle between the two data samples in the cross-correlation, D_1R_2 and D_2R_1 are the number of pairs between the data and samples of random points, and R_1R_2 are pairs between the two random samples. If there is no position-dependent selection function, the random catalogues are only required to follow the same geometry as the data catalogues. It should be noted that for autocorrelations $1 = 2$ but we generalize for cross-correlations. This and similar estimators are designed to measure excess densities relative to a random distribution of points. By having the random samples mimic the density variations due to the selection function, we can remove these contributions from the correlation. In the above equation, R_1 would ideally have the same selection efficiency as D_1 and likewise for R_2 and D_2. It is advantageous to weigh the random samples instead of the data

samples because this approach decreases shot noise and maps the full selection function rather than just at points sampled by the galaxies.

These random points are difficult to construct both analytically and empirically as they require a mapping of the values of the systematics to the expected under- and overdensities. Analytically determining the mapping of systematics to the induced selection requires an understanding of how the systematics affect the selection of the galaxy sample considered. This is only possible for the simplest of selections and becomes impossible without large assumptions when the selection criteria are complex and the systematics numerous. In principle, one could attempt to simulate the data and selection process that results in the systematics variations. However, this would require complex end-to-end simulations of the full galaxy sample, reduction- and detection-pipeline, multicolour photometry, photo-z, etc.

Determining the weighting empirically (or blindly) through mapping galaxy density to the set of systematics values is a more realistic option for complex selections. We can measure the value of each systematic at every position in the survey and map it to the observed density. This is the approach we take and it works well as long as there is a sufficient density of galaxies to map out the dependence. Once the galaxy sample drops below $\sim$1 gal arcmin^{-1} in CFHTLenS the fidelity of the map suffers. Another difficulty is if our knowledge of the systematic does not have a fine enough resolution to probe the scales of interest or is contaminated (as in the case of the stellar density discussed above). In this paper, we find that with the majority of galaxy samples we are able to fit for much of the systematic variation.

5.2 Data preparation

Creating a weighted masking for a photometric data set such as CFHTLenS is complicated and requires careful consideration. This is mainly due to the large volume of data and the numerous possible systematics making determining the weighting challenging if the galaxy sample under consideration is sparse and the effect is small. The problem is to estimate the density of galaxies as a function of 11 variables making this a very high-dimensional problem.

Throughout this analysis, we utilize the spherical pixelization code STOMP and follow a methodology similar to Scranton et al. (2002) to create the maps of systematics as a function of position and compute the correlations. We start by describing how the data are prepared, moving on to the smoothing of the data and then the creation of the weight maps.

We utilize the STOMP maps created and described previously in Section 2 to map the positional dependence of both the survey systematics and galaxy densities. Specific to our analysis of CFHTLenS, we use relative values of the density and systematics compared to the mean of each pointing instead of the global mean of the survey. This increases the signal to noise of our estimates in CFHTLenS (see Fig. 3). In order to properly estimate the density of galaxies against the systematics, we must find a way to bin the data such that the bins capture much of the variation in the systematics but contain enough galaxies to properly estimate their density. This is a classical problem in high-dimensional data analysis and requires an algorithm to efficiently map the parameter space and group data points. To do this, we utilize a k-means clustering approach to identify portions of the data that have similar systematics values across pointings and estimate the galaxy density in these clusters.

5.3 k-means clustering

Binning high-dimensional data efficiently is a non-trivial problem. We use a k-means clustering method (MacQueen 1967) in order to bin survey pixels with similar systematic values and compute an average of the sample galaxy density contained in those pixels. In general, this machine learning algorithm aims to locate portions of the data with equal variance and bin them into clusters. The algorithm attempts to minimize

$$\sum_{i=1}^{k} \sum_{x_j \in S_i} \| x_j - \mu_i \|, \tag{3}$$

where μ_i is the ith cluster mean, the point x_j is a member of the set S_i of all points nearest to μ_i, the first sum is carried out over all k clusters, and the second sum is carried out over all points in the ith cluster. Cluster centres are initially chosen at random. The centre is then updated using the mean of the nearest data points. The process is repeated until the difference in the sum above for new centres from one iteration to the next reaches a convergence criterion. We pick this method due to the ease of attributing new values to the already determined clusters and the simplicity of interpolating as a function of distance from cluster centres. We use the MiniBatchKMeans method from the scikit-learn PYTHON package[4] designed for fast convergence on large data sets with a high dimensionality.

As this technique is minimizing the variance of the clusters, we normalize the variance of each systematic considered to unity, that is, each value of the systematics is normalized by

$$z(\boldsymbol{\theta}) = \frac{s(\boldsymbol{\theta}) - \langle s_i \rangle}{\sigma(s(\boldsymbol{\theta}) - \langle s_i \rangle)}, \tag{4}$$

where z is the normalized value of the systematic at position $\boldsymbol{\theta}$, s is the original value of the systematic, $\langle s_i \rangle$ is the average value of the systematic in pointing i containing $\boldsymbol{\theta}$, and $\sigma(s(\boldsymbol{\theta}) - \langle s_i \rangle)$ is the standard deviation of the systematic minus the pointing mean over the full survey. The k-means algorithm then considers each dimension equally rather than overfitting certain variables due to their small variance. This allows the method to fit the systematics without any assumption about the galaxy sample's sensitivity to a given systematic. On application to the CFHTLenS data set the number of clusters we use varies with the density of the galaxy sample. We use three different numbers of clusters: 64, 128, 256, which are arbitrarily chosen but span the range of under and overfitting the variations in data when removing the systematics. We then calculate the average overdensity and errors in each k-means cluster by spatially jackknifing over each of the $\leq$171 pointings of CFHTLenS contributing to the cluster.

5.4 Testing

We use the mapping of systematics to densities that comes out of the k-means clustering approach as a weighting from which to draw random samples. We can test the success of our weighting scheme by comparing the cross-correlations of the galaxy samples under consideration against each of the different systematics maps both before and after the weighting is applied. If the correction has worked, the correlation between the galaxy samples and the systematics maps should equal the correlation between the weight maps and the systematic maps within shot noise errors. This is a result independent of the science goal. The difference between

[4] http://scikit-learn.org/

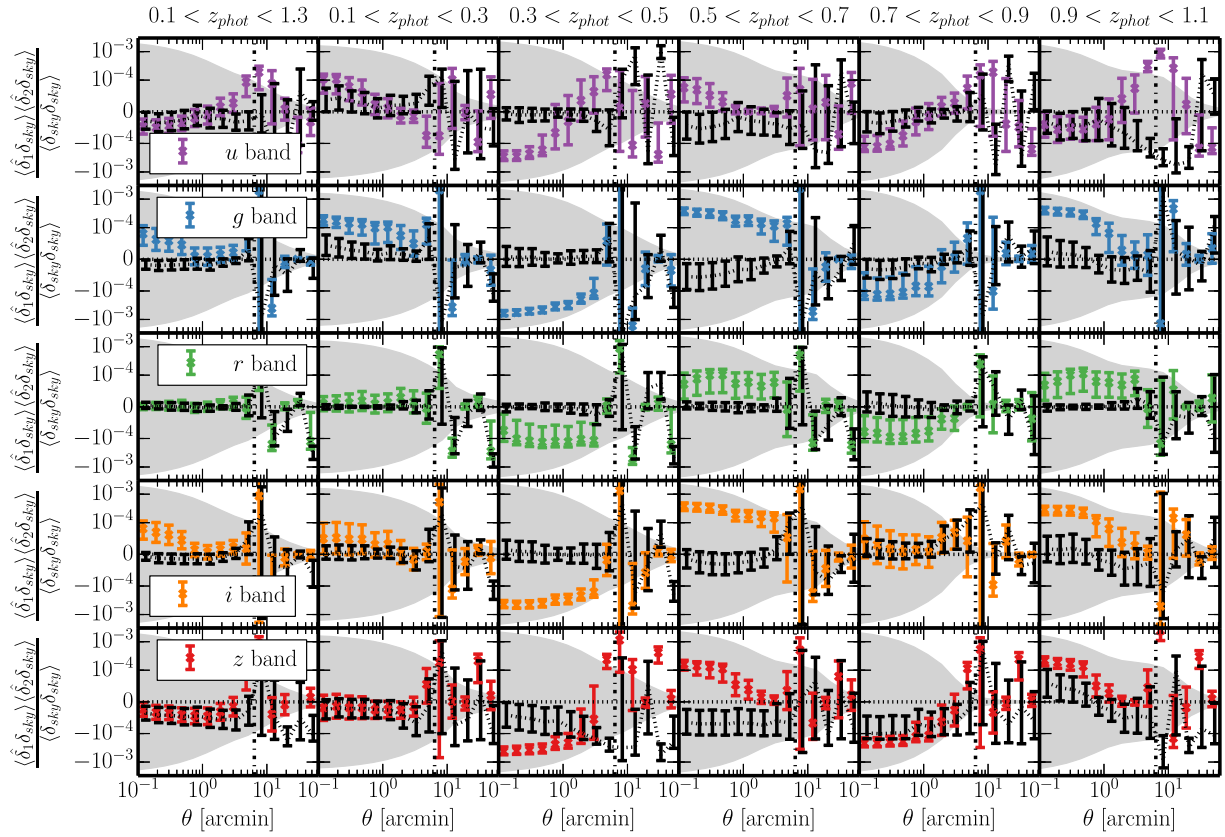

Figure 13. Symmetric log plots of the observed and corrected depth systematics for foreground lens galaxies cross-correlated against the u'-dropout sources. The y-axis is plotted linearly for the range $\pm 10^{-4}$. The quantity plotted on is the estimated contribution from the depth to the magnification cross-correlation assuming linear systematics only. Unconnected x's show the raw systematic contamination. The black dashed line is the estimated correlation after the correction is applied again assuming linear systematics. Columns show these correlations for the different photo-z-selected samples and the rows show the correlations against the different bands. The dark shaded region is ± 10 per cent of the expected magnification signal for the photo-z sample (assuming a galaxy bias of $b = 1$) lensing the u-dropout sample (assuming a slope of the number counts of $\langle \alpha - 1 \rangle = 1$).

these two correlations yields an unbiased estimate of the amount of residual systematic error in the measurement after the weighting has been applied. It also gives an objective criterion to discard samples that cannot be properly corrected using this method as it shows they have more issues with possibly unknown systematics than can currently be accounted for. These tests are also independent of cosmology or any assumptions pertaining to the galaxy sample as long as just instrumental and galactic systematics are considered.

6 RESULTING CORRECTIONS

Here, we present results from modelling the relation of galaxy density against the 11 different systematics determined from our k-means method. We show how well the weights we create remove the systematic compared to the amount of systematic correlation we see before and after the correction is applied. We do this in a manner similar to Ho et al. (2012) where the expected correlation amount for our cross-correlation is

$$\langle \delta_1 \delta_2 \rangle_{\mathrm{sys}_{ij}} \sim \frac{\langle \delta_1 \delta_{\mathrm{sys}_i} \rangle \langle \delta_2 \delta_{\mathrm{sys}_j} \rangle}{\langle \delta_{\mathrm{sys}_i} \delta_{\mathrm{sys}_j} \rangle}, \tag{5}$$

where $\langle \delta_1 \delta_2 \rangle_{\mathrm{sys}_{ij}}$ is the contribution from systematics i, j contributing to the galaxy cross-correlation, $\delta_{1/2}$ is the overdensity of galaxies for samples 1 and 2, respectively, and δ_{sys_i} is the ith systematic considered. This equation is only truly valid for linear correlations and is likely not completely valid for the scales we consider. However, it does give us some indication of success. This is the best we can do currently without observing the galaxy cross-correlation before and after correction. This could add confirmation bias as we may stop once this galaxy cross-correlation looks 'correct'. The plots shown in this section are only for the cases where $i = j$. The cross-terms are left out of the paper for brevity but are observed to be as improved as the diagonal terms.

As an application of this method we compare the residual systematic correlation signal to the expected signal from weak lensing magnification bias. We determine that we have successfully mitigated the systematic if the majority of the corrected correlations are consistent to within 10 per cent of the expected magnification signal and that we see a reduction in amplitude for each correlation. It is clear that such a criterion does not directly guarantee that the correlation functions used in the science analysis are free from any systematics. However, it is a necessary criterion to assure that none of the systematics investigated here swamp the signal.

Fig. 13 shows the cross-correlation amplitude between the lens galaxy samples and the u-dropouts sample caused by the systematics (unconnected coloured x's) and this same systematic correlation after the weighted correction is applied. This difference is shown by the black data points connected by the dotted line. The dark shaded region in each plot represents our criterion of 10 per cent of the magnification bias signal expected from a cross-correlation of the photo-z sample and a source sample at $z = 3$. For this signal, we also have to assume some value for the slope of the source number

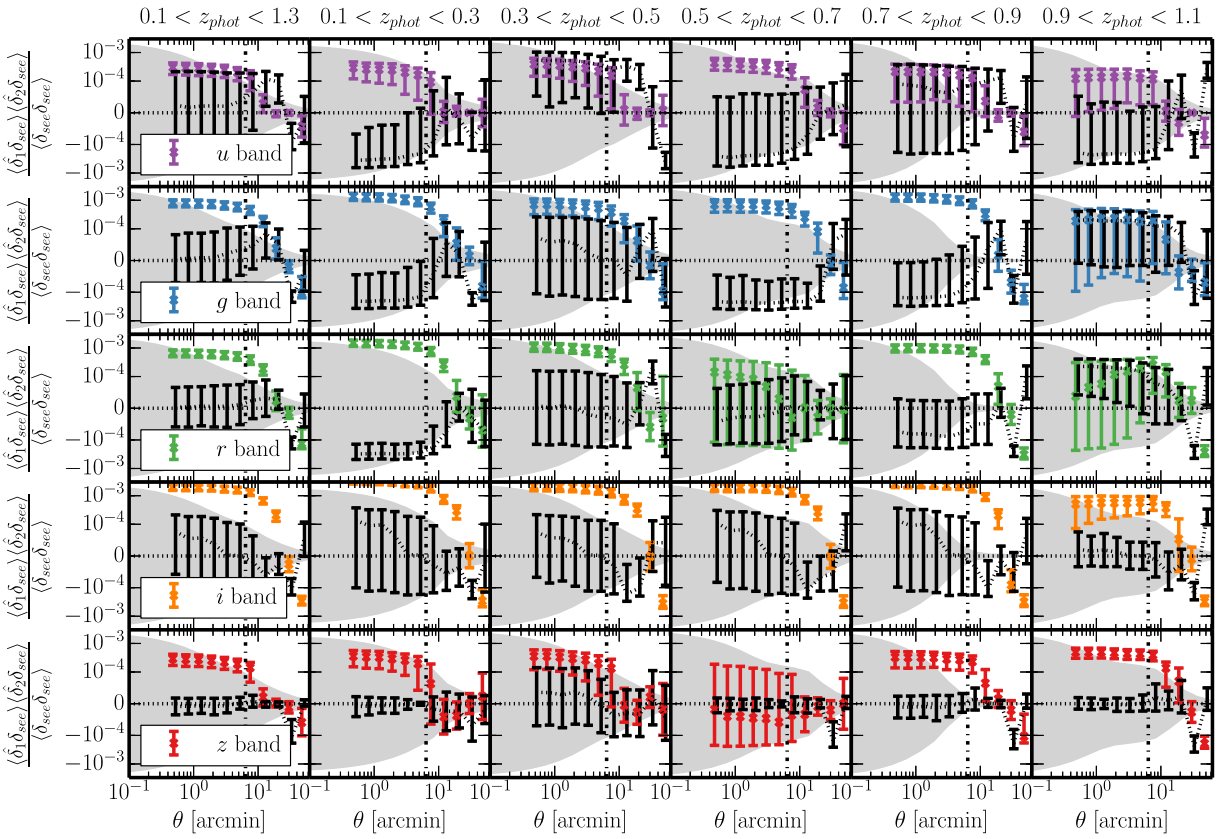

Figure 14. Same as Fig. 13 but showing the correlations against the PSF FWHM maps instead of the survey depth.

counts and here we choose this to be $\langle \alpha - 1 \rangle = 1$.[5] Additionally, we assume a galaxy bias of $b = 1$ for the foreground sample.

For the contribution from the depth, the photo-z-selected samples with redshifts $z_{\rm phot} < 0.9$ and the global redshift sample ($0.1 < z_{\rm phot} < 1.3$) correlated against the u-dropout sample are mostly consistent with the 10 per cent criterion. For higher redshifts this is not the case, especially in the u band. The $0.3 < z_{\rm phot} < 0.5$ and $0.5 < z_{\rm phot} < 0.7$ correlations show the most marked improvement, where the amplitudes before correction are the largest of all of photo-z samples and the amplitude after correction is reduced to a level consistent with zero at small scales ($\theta < 5$ arcmin) for all but the z band. In general, all the correlations are consistent with zero after correction at scales $\theta < 10$ arcmin. At large scales it is difficult to interpret the results due to the noise in these bins at the edge of the survey pointings.

For the higher redshift slices, the improvement is not as dramatic. The $0.9 < z_{\rm phot} < 1.1$ sample shows that correlations versus the survey depth are improved in all bands except for the u band which retains a large coherent amplitude at $\sim$10 arcmint. Explaining this discrepancy is difficult considering the marked improvement in the other four bands. It is likely due to this sample being significantly fainter and sparser than the other samples considered. This both makes the systematics more severe due to the faintness and their effect harder to estimate due to the sparseness of the sample.

The improvements seen for the low $z_{\rm phot}$ cross-correlations comes from both the foreground lens and source u-dropout LBGs. The LBGs show the largest correlations for all the systematics, especially the u-dropout sample. These source samples show improvements by an order of magnitude from what is observed in Figs 6, 9, and 12 and are a large part of the improvement seen when combined with the foreground. The results shown here are similar for the g dropouts which are left out of this section for brevity.

Fig. 14 shows the correlations and corrections against the seeing for the photo-z-selected and LBG samples. We utilize the same empirically estimated density map as in the previous figures which is simultaneously correcting for all the considered systematics. The systematics observed here are roughly on the same order as the depth systematics with more of the seeing systematic correlation amplitudes being outside of our criteria. After correction, the correlation amplitudes show marked improvement with the z- and i-band being consistent with zero. The other bands are slightly less successful but are made consistent with our criteria.

Fig. 15 shows the extinction map correlated against the different CFHTLenS galaxy samples and the corrected correlations. Modelling of this systematic is the least successful, though for the lower redshift ($z_{\rm phot} < 0.9$) galaxies the amplitude is reduced by an order of magnitude for most samples. One possible reason for this is that the extinction is the only variable considered that is contaminated by signal from large-scale structure. The $E(B-V)$ extinction maps are in part determined by infrared emission and partly contaminated by emission from the CIB as shown in e.g. Schmidt et al. (2015).

Overall, we find encouraging results in modelling and removing the largest systematics, reducing much of the spurious signal from the 11 systematics considered to consistent with zero for the expected contribution to the signal from systematics. This is largely true for the lower redshift bins, i.e. samples with $z_{\rm phot} < 0.9$. For

[5] This is a conservative value for both dropout samples which are measured to have a slightly higher value (Hildebrandt et al. 2009b).

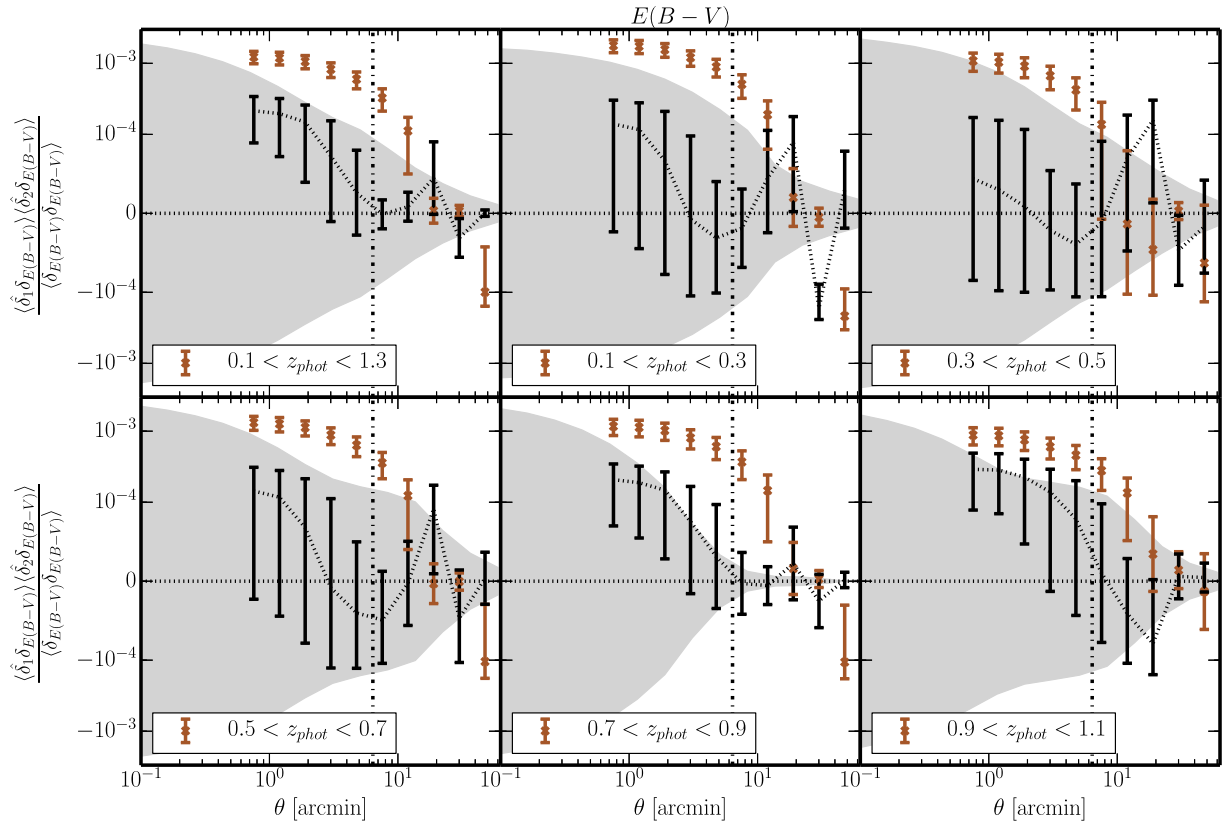

Figure 15. Similar to Fig. 13 but for correlations against the $E(B-V)$ map as derived from the SFD dust maps(Schlegel et al. 1998). For these plots, each separate panel is for a different galaxy sample.

higher photo-z slices, the corrections and modelling tend to break down. This is likely due to the increased sparseness and faintness of these samples with the mean magnitude shifting by one magnitude in the most extreme case. These samples also have less that 1/3rd of the galaxies as the number of lower redshift samples. These faint samples are much more susceptible to the effect of systematics and it is likely there is not enough data to constrain these effects. We find more success with the LBG samples likely due to the simple nature of the colour–colour selection. Large-scale corrections can be problematic for some samples though this is difficult to interpret due to noise. This is likely due to smoothing we perform, treating each pointing individually rather than the whole survey simultaneously.

7 DISCUSSION AND CONCLUSIONS

In this paper, we have presented an investigation into systematic density variations of galaxy samples in CFHTLenS caused by variations of instrumental and astrophysical quantities. We also present a model that attempts to mitigate these effects, empirically modelling galaxy density as a function of survey systematics. We model these survey systematics with an eye towards measuring magnification in CFHTLenS and other similar multi-epoch, wide area surveys. We consider survey systematics of limiting magnitude (depth), PSF size (FWHM), and galactic extinction ($E(B-V)$). In total for CFHTLenS this is 11 systematic variables: five depth, five PSF sizes, and one extinction. We find that, without a correction, correlations induced by variations in such systematics can be significant compared to the intended measurement. We find induced density fluctuations in small fractions of the area of the survey of up to 10 per cent in photo-z-selected samples and up to even 50 per cent in high-z LBG samples. This can result in correlation amplitudes of 0.1 and 1.0 per cent, respectively. In the case of magnification bias, this spurious correlation can be as large as twice the expected amplitude of the signal one wants to measure!

We modelled these systematics by identifying regions of similar systematic values in the survey (in the 11 dimensions mentioned above) using a k-means clustering approach and estimating the average galaxy overdensity as a function of the survey systematics. Using this method, we see improvement in the spurious cross-correlation systematics for the majority of the galaxy samples considered. In some cases, the weighted correction reduces the expected contribution from systematics such that it is consistent with zero. The high redshifts, unfortunately, do not improve considerably and still show significant correlation of similar amplitude to the magnification. This is likely due to the large difference in brightness of the samples, with the higher redshift samples being much fainter and sparser. These fainter samples are then more sensitive to selection effects and, due to these samples being sparser and noisier, we are unable to effectively estimate a correction with high precision.

The LBG samples considered are an exception. While they are the faintest and sparsest samples that we are trying to correct, their corrections work surprisingly well. This is likely due to the fact that the LBGs are selected with simple, two-dimensional colour cuts. The high-z photo-z samples in contrast are selected in a much more complicated way by the inner workings of a photo-z code (BPZ in our case) so that it is conceivable that their dependence on systematics is also more complicated.

The analysis presented here directly enables measurements of magnification bias in the CFHTLenS. In the future, we will apply

this technique to other surveys such as RCSLenS and KiDS. These surveys are very similar to CFHTLenS (especially in terms of data processing) and will enable quick turn around on the science.

This technique will benefit from larger area, deeper future surveys, however, care will need to be taken to assure that computation time is tractable. The *k*-means algorithm used in this work is designed for large data sets and will likely scale properly though further investigation is needed. In order to proceed with these larger data sets and properly remove systematics down to smaller scales, simulations of the data set mimicking the observing strategy and large-scale structure will be required. This will give an understanding of both density dependence on survey systematics, but also systematics from changes in densities caused by deblending and light haloes. This method could then be trained with simulated catalogues that mimic the systematics probed. This is left for future work.

The fundamental limitation of this technique is the finite size of the galaxy sample that is used to map the dependence on the different systematics. While larger surveys will contain more information to establish this relation those surveys will also require systematic errors to be controlled to a higher level. It is not clear at the moment which of the two aspects will win in the end, i.e. whether our ability of modelling systematic effects will scale more favourably with increasing data volume than statistical noise or the opposite.

ACKNOWLEDGEMENTS

We thank Peter Schneider for his valuable feedback. We also thank our referee, Enrique Gaztanaga for his helpful comments and suggested improvements of the manuscript. CM and HH are supported by the DFG Emmy Noether grant Hi 1495/2-1.

This work is based on observations obtained with MegaPrime/MegaCam, a joint project of CFHT and CEA/IRFU, at the Canada–France–Hawaii Telescope (CFHT) which is operated by the National Research Council (NRC) of Canada, the Institut National des Sciences de l'Univers of the Centre National de la Recherche Scientifique (CNRS) of France, and the University of Hawaii. This work is based in part on data products produced at TERAPIX and the Canadian Astronomy Data Centre as part of the Canada-France-Hawaii Telescope Legacy Survey, a collaborative project of NRC and CNRS. This research used the facilities of the Canadian Astronomy Data Centre operated by the National Research Council of Canada with the support of the Canadian Space Agency. CFHTLenS data processing was made possible thanks to significant computing support from the NSERC Research Tools and Instruments grant programme.

REFERENCES

Bauer A. H., Seitz S., Jerke J., Scalzo R., Rabinowitz D., Ellman N., Baltay C., 2011, ApJ, 732, 64
Bauer A. H., Gaztañaga E., Martí P., Miquel R., 2014, MNRAS, 440, 3701
Benítez N., 2000, ApJ, 536, 571
Bertin E., Arnouts S., 1996, A&AS, 117, 393
Erben T. et al., 2005, Astron. Nachr., 326, 432
Erben T. et al., 2013, MNRAS, 433, 2545
Ford J. et al., 2012, ApJ, 754, 143
Ford J., Hildebrandt H., Van Waerbeke L., Erben T., Laigle C., Milkeraitis M., Morrison C. B., 2014, MNRAS, 439, 3755
Heymans C. et al., 2012, MNRAS, 427, 146
Hildebrandt H., Pielorz J., Erben T., van Waerbeke L., Simon P., Capak P., 2009a, A&A, 498, 725
Hildebrandt H., van Waerbeke L., Erben T., 2009b, A&A, 507, 683
Hildebrandt H. et al., 2011, ApJ, 733, L30
Hildebrandt H. et al., 2012, MNRAS, 421, 2355
Hildebrandt H. et al., 2013, MNRAS, 429, 3230
Ho S. et al., 2012, ApJ, 761, 14
Huff E. M., Graves G. J., 2011, preprint (arXiv:1111.1070)
Landy S. D., Szalay A. S., 1993, ApJ, 412, 64
Le Fèvre O. et al., 2005, A&A, 439, 845
Leistedt B., Peiris H. V., 2014, MNRAS, 444, 2
Leistedt B., Peiris H. V., Mortlock D. J., Benoit-Lévy A., Pontzen A., 2013, MNRAS, 435, 1857
MacQueen J., 1967, Some Methods for Classification and Analysis of Multivariate Observations. Univ. California Press, Berkeley, CA, p. 281
Ménard B., Bartelmann M., 2002, A&A, 386, 784
Ménard B., Scranton R., Fukugita M., Richards G., 2010, MNRAS, 405, 1025
Miller L. et al., 2013, MNRAS, 429, 2858
Morrison C. B., Scranton R., Ménard B., Schmidt S. J., Tyson J. A., Ryan R., Choi A., Wittman D. M., 2012, MNRAS, 426, 2489
Newman J. A. et al., 2013, ApJS, 208, 5
Planck Collaboration XI, 2014, A&A, 571, A11
Ross A. J. et al., 2012, MNRAS, 424, 564
Schlegel D. J., Finkbeiner D. P., Davis M., 1998, ApJ, 500, 525
Schmidt F., Leauthaud A., Massey R., Rhodes J., George M. R., Koekemoer A. M., Finoguenov A., Tanaka M., 2012, ApJ, 744, L22
Schmidt S. J., Ménard B., Scranton R., Morrison C. B., Rahman M., Hopkins A. M., 2015, MNRAS, 446, 2696
Scranton R. et al., 2002, ApJ, 579, 48
Scranton R. et al., 2005, ApJ, 633, 589
van Waerbeke L., 2010, MNRAS, 401, 2093

This paper has been typeset from a TEX/LATEX file prepared by the author.